Interactions between particles and quantized vortices in superfluid helium

Demosthenes Kivotides,[1] Carlo F. Barenghi,[2] and Yuri A. Sergeev[3]
[1]*Center for Risk Studies and Safety, Dept. of Chemical Engineering, University of California, Santa Barbara, California 93117, USA*
[2]*School of Mathematics and Statistics, Newcastle University, Newcastle upon Tyne, NE1 7RU, United Kingdom*
[3]*School of Mechanical and Systems Engineering, Newcastle University, Newcastle upon Tyne, NE1 7RU, United Kingdom*
(Received 18 June 2007; revised manuscript received 31 August 2007; published 28 January 2008)

We present a numerical, computational, and physical analysis of particle-vortex collisions in thermal superfluids. Our method allows fully self-consistent, dynamic computation of particle-vortex collisions within the vortex dynamical formalism. The algorithm is described in detail and is shown to be both accurate and efficient. The method is applied to the collision of a solid particle with a straight vortex at finite temperature. It predicts that the smallest velocity that the approaching particle must have in order to escape the vortex after being captured by it increases as the temperature approaches the superfluid transition temperature. A comparative study of particle-vortex collisions at various temperatures reveals the contributions of viscous damping, inertial, and boundary-induced effects on the dynamics of the system, as well as different particle-vortex interaction behaviors. The findings corroborate the possibility of direct measurement of the normal fluid velocity in thermal superfluids via appropriately designed particle image velocimetry experiments.

DOI: 10.1103/PhysRevB.77.014527 PACS number(s): 67.25.dk, 47.37.+q, 47.55.Iv

I. INTRODUCTION

Thermal superfluid hydrodynamics[1–3] poses many challenging and intriguing physics problems. From the theoretical point of view, fundamental difficulties arise from the need of an adequate mathematical treatment of the interaction of two nonlinear, three-dimensional mechanical fields representing the normal-fluid and superfluid components. In general, thermal superfluids are in a turbulent state and their mathematical study is very demanding; due to the complexity of turbulence, numerical computations are only possible for small Reynolds numbers.[4–6] Therefore experimental evidence is expected to play a crucial role in understanding superfluid hydrodynamics. However, until recently, little experimental information has been made available of normal-fluid and superfluid flow patterns, let alone of simultaneous direct measurement of superfluid and normal-fluid velocities and spectra.

Recently, a number of experiments have been performed[7,8] that tried to address this data shortage. The idea behind these experiments is to release micron-sized solid particles in the flow, which can be imaged with a laser to determine their velocity or patterns. However, this technique has created the problem of interpreting the images of particles in terms of flow velocities or vorticity. This problem has motivated theoretical efforts to understand the motion of particles in superfluids. A by-product of the latter investigation is a better understanding of the[7,8] experiments, and the design of new, more informative experiments. Initially, Poole *et al.*[9] formulated a mathematical model of multiphase thermal superfluids in which the particle motion does not affect the flow of either of the fluids. The model assumes that the particle diameter is much smaller than the smallest scale of flow variation in both fluids in order to describe the particle dynamics via asymptotically valid differential equations. This assumption is violated, however, when a particle collides with a superfluid vortex, since the latter is characterized by a nanometer-sized vortex core which is always orders of magnitude smaller than the particles diameter. Because of this restriction, Kivotides *et al.*[10] had to confine themselves to thermal superfluids with a small density of superfluid vortices and a dilute system of particles; under these restrictions particle-vortex collisions are not important, and they were able to show that viscous drag enforces the particles to move with the normal-fluid velocity. We note in passing that they found that the mutual-friction induced[10] normal-fluid flow around a superfluid vortex deflects approaching particles, and so obstructs direct particle-vortex collisions. However, since the latter effect was predicted by the equations of Ref. 9 that ignore the "corrections" to particle motion induced by the accompanying self-consistent vortex deformation during close encounters, and moreover, since Kivotides *et al.*[11] have shown that in counterflow situations such close encounters are unavoidable, it became evident that a more powerful computational methodology had to be developed.

As a start,[12] following a research approach initiated by Ref. 13, Kivotides *et al.* developed a computational procedure for calculating how the presence of particles affects superfluid vortex dynamics (VD). The method of Ref. 12 has two drawbacks: (a) it cannot treat vortex-particle collisions, and (b) it is not fully dynamic, since the particle motion has to be kinematically prescribed. The present contribution removes these drawbacks enabling dynamical calculations of vortex-particle collisions. It ought to be mentioned that Refs. 14 and 15 have successfully computed collisions of vortices with particles. The latter, however, were either stationary or moving with kinematically prescribed velocities. Self-consistent evolutions are calculated here.

II. MATHEMATICAL PROBLEM

The most general formulation of our problem would be the interaction between N_p spinning, buoyant, finite-size, dynamic shaped particles and N_v vortex loops under suitable boundary conditions. In this form our problem would be quite complex and (in principle) would be only solved ap-

proximately with (as yet undeveloped) numerical and computational methods. Indeed, whole monographs can be exclusively devoted to the study of a pure particle[16] or pure vortex[17] subproblems. However, if we confine ourselves to the study of a $N_p=1$ spinless, neutrally buoyant (i.e., the Archimedean force exactly cancels the gravitational force on the particle), spherical particle interacting with N_v vortices in infinite space domain, we can take advantage of the explicit equation of motion of one particle in a system of superfluid line vortices developed by Schwarz.[13] In this way, there is also no need to specify how the particles collide, i.e., whether they are elastic (conserving kinetic energy during collisions) or viscoelastic (dissipating kinetic energy to heat during collisions). Hereafter, in accordance with the spinless particle assumption, we consider only linear momentum dynamics, ignoring any angular momentum effects.

In particular, let $\mathbf{X}(l,t)$ denote the superfluid vortex link $\mathcal{L}$ where l is the arclength parametrization along the vortex loops (knots) and t is time. The evolution equation for $\mathbf{X}(l,t)$ is given by

$$\frac{\partial \mathbf{X}}{\partial t} = \mathbf{V}^s + \mathbf{V}^b + \mathbf{V}^\phi + \mathbf{V}^f. \tag{1}$$

The first contribution is the superfluid velocity $\mathbf{V}^s$ is given by the Biot-Savart integral:

$$\mathbf{V}^s(\mathbf{x}) = -\frac{\kappa}{4\pi}\int_{\mathcal{L}} dl \frac{\mathbf{X}' \times (\mathbf{X}-\mathbf{x})}{|\mathbf{X}-\mathbf{x}|^3}, \tag{2}$$

where $\mathbf{X}' \equiv \partial \mathbf{X}/\partial l$ is the unit tangent vector (indicating the direction of the singular superfluid vorticity) and κ is the quantum of circulation. The second contribution $\mathbf{V}^b$ denotes the "deformation" of free vortex dynamics due to the presence of a stationary particle at a particular location inside the flow. Its calculation follows from the requirement that the effect of the particle on the vortices must be such that the combined (i.e., vortical plus particle induced) flow field on the particle's surface has an identically zero radial component. It is convenient to write $\mathbf{V}^b$ as the gradient of a scalar field Φ^b, i.e., $\mathbf{V}^b \equiv \nabla \Phi^b$. This follows from a well-known theorem of vector analysis that states that in a simply connected space region, every irrotational vector field is also a conservative vector field. Indeed, since we do not model the superfluid with the Gross-Pitaevskii equation, our fluid domain is simply connected (i.e., there are no voids at the center of the vortices). Moreover, since the superfluid is inviscid, the presence of the sphere does not generate a vortical (rotational) boundary induced field $\mathbf{V}^b$. Thus both conditions of the aforesaid theorem are valid for field $\mathbf{V}^b$, and no restricting hypothesis is involved. Because of the incompressibility condition, the Φ^b satisfies the Laplace equation:

$$\nabla^2 \Phi^b = 0. \tag{3}$$

$\mathbf{V}^b$ satisfies the boundary condition:

$$(\mathbf{V}^s + \mathbf{V}^b) \cdot \hat{\mathbf{n}} = 0, \tag{4}$$

with $\hat{\mathbf{n}}$ denoting the unit radial vector field on the spherical particle surface. The latter is defined as the set of points $\mathbf{x}$ satisfying the condition $|\mathbf{x}-\mathbf{z}|=a$, with a being the radius of the particle and $\mathbf{z}$ being the particle's center.

The third contribution $\mathbf{V}^\phi$ is the potential flow field induced by the motion of a spherical particle with velocity $\mathbf{V}^p$. This flow field is given by the expression[18]

$$\mathbf{V}^\phi(\mathbf{x},t|\mathbf{z}) = -0.5\left(\frac{a}{r}\right)^3 \mathbf{V}^p(\mathbf{z}) \cdot \left(\mathbf{I} - 3\frac{\mathbf{x}'\mathbf{x}'}{r^2}\right), \tag{5}$$

where $\mathbf{V}^\phi(\mathbf{x},t|\mathbf{z})$ is the velocity of the fluid at $\mathbf{x}$ caused by a sphere of radius a whose center is located at $\mathbf{z}$, $\mathbf{I}$ is the 3×3 unit matrix whose elements are the Kronecker symbols δ_{ij} $(i,j=1,2,3)$, $\mathbf{x}'=\mathbf{x}-\mathbf{z}$, and $r=|\mathbf{x}-\mathbf{z}|$.

Finally, the fourth term is the mutual friction associated velocity $\mathbf{V}^f$ given by a formula derived in Ref. 19:

$$\mathbf{V}^f = h_{\star\star}(\mathbf{V}^s + \mathbf{V}^b + \mathbf{V}^\phi) + h_\star \mathbf{X}' \times [\mathbf{V}^n - (\mathbf{V}^s + \mathbf{V}^b + \mathbf{V}^\phi)] + h_{\star\star}\mathbf{X}' \times (\mathbf{X}' \times \mathbf{V}^n), \tag{6}$$

where $\mathbf{V}^n$ is the kinematically prescribed normal fluid velocity, and $h_\star = d_{\star\star}/[d_{\star\star}^2 + (1-d_\star)^2]$, $h_{\star\star} = (d_\star - d_{\star\star}^2 - d_\star^2)/[d_{\star\star}^2 + (1-d_\star)^2]$ are dimensionless numbers given in terms of the (also dimensionless) mutual friction coefficients $d_\star$ and $d_{\star\star}$. To compute the latter coefficients, one starts from the Hall-Vinen coefficients and following Ref. 20 calculates the transverse and longitudinal drag coefficients $D'_\star$ and $D_{\star\star}$. Subsequently, one computes $D_\star = D'_\star - \rho_n\kappa$, and finally $d_\star = D_\star/(\rho_s\kappa)$, $d_{\star\star} = D_{\star\star}/(\rho_s\kappa)$. It is noted that in the single-phase superfluids literature, methods have been developed for the computation of fully dynamical thermal superfluids evolutions.[21] However, these methods are not directly applicable to multiphase thermal superfluids, since the latter require the accurate computation of the flow at the solid–normal-fluid interface. This task could be achieved in the future using either the "diffuse interface method" (also known as "immersed boundary method")[22] or the "sharp interface method".[23]

The particle equation of motion is an equation derived by Schwarz in Ref. 13 with the addition of a viscous damping force. It reads:

$$m_e \frac{d\mathbf{V}^p}{dt} = 6\pi a \mu_n (\mathbf{V}^n - \mathbf{V}^p) + 2\pi\rho_s a^3 \frac{\partial \mathbf{V}^s(\mathbf{z},t)}{\partial t} + \frac{1}{2}\rho_s \int_S dS (\mathbf{V}^s + \mathbf{V}^b)^2 \hat{\mathbf{n}}, \tag{7}$$

where m_e is the effective mass of the particle $m_e = m + (2/3)\pi\rho_s a^3$, m is the particle mass, μ_n is the dynamic viscosity of the normal fluid, ρ_s and ρ are the superfluid mass density and total mass density, respectively, and $\mathbf{V}^s(\mathbf{z},t)$ is the vortex-induced velocity at the particle center; the last term is a surface integral with $\hat{\mathbf{n}}$ being the outward unit radial vector field on the spherical particle surface. It is convenient to write the right-hand side of Eq. (7) as $\mathbf{f}=\mathbf{f_d}+\mathbf{f_l}+\mathbf{f_b}$, this decomposes the total force $\mathbf{f}$ into viscous drag, $\mathbf{f_d}$, local, $\mathbf{f_l}$, and boundary force, $\mathbf{f_b}$. Equation (7) takes into account the effect of the normal-fluid on particle motion via a viscous drag force known as Stokes force (first term on the right-hand side). We have set $\mathbf{V}^n \equiv \mathbf{0}$ throughout this investigation.

Equation (7) is a very elementary model of a particle moving within a thermal superfluid because it does not include many (potentially important) physical effects. For example, the last two terms on the right-hand side represent an exact and complete treatment of the particle force only for pure superfluids. At finite temperatures, there must be additional terms that take into account the fact that, due to the mutual friction, superfluid flow cannot be treated as a simple incompressible potential flow. In addition, our system of differential equations does not take into account the effects on the motion of superfluid vortices of particle induced normal-fluid flow. The treatment of these and other similar effects requires a more sophisticated numerical and computational method that could be developed in the future. Such a method would allow the study of refined physical effects which occur in situations where all three components (superfluid, normal-fluid, particle-field) exhibit strongly interacting, fluctuating behavior. These situations could be important for theoretical, as well as experimental reasons, and their study could also benefit other branches of physics.

In summary, in order to understand particle-vortex interactions in the framework of the present model, one has to solve the coupled system of integrodifferential equations (1) and (7). The solution of Eq. (1) requires the solution of the subproblem (3) and (4). However, there is still a serious gap in this formulation: it is expected that particles tend to collide with vortices, but the physics of such encounters are not included in Eq. (1). An equation that encompasses such a process is the Gross-Pitaevskii (GP) equation for a Bose-Einstein condensate that has already been used for studying a problem similar to ours but of atomic scale.[24] Although, in principle, the GP equation could describe the interaction of micron-sized particles with vortices in "large" (centimeter-sized) fluid systems, in practice, the computational complexity required to "bridge" the nanometer-scale phenomena at the vortex core level with the centimeter-scale flow phenomena in the bulk forbids such a computation. Therefore since our purpose is to establish contact between theory and experiments, we are forced to employ VD. In the next section, we present a method for particle-vortex collision in the context of the VD formalism. Our method is an extension to the case of moving particles of the methodology that was developed in Ref. 14 for the case of stationary particles.

III. SOLUTION METHODS

A. Reconnection-free evolution

The coupled system of integrodifferential equations (1) and (7) is solved using a third order accurate, low storage Runge-Kutta (RK) method. This approach requires the discretization of the Biot-Savart integral in the fashion of Riemann sums. The desingularization of the kernel is achieved by splitting it into local and nonlocal parts. According to the method of Schwarz,[14] the local contribution is equal to the propagation velocity of a vortex ring with radius equal to the local radius of curvature. The nonlocal contribution is computed by employing a Gaussian kernel in order to smooth the singular superfluid vorticity. The numerical analysis of this method has been described by Winckelmans and Leonard.[25]

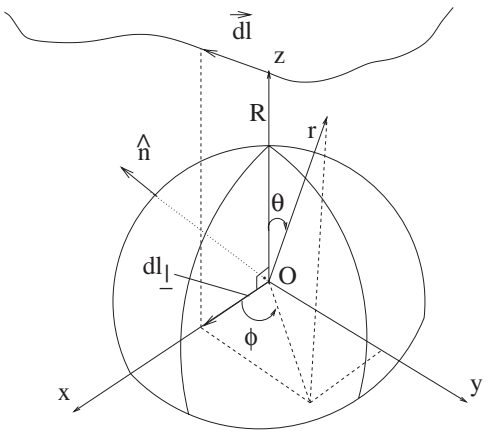

FIG. 1. Coordinate system and variables used in the numerical formulas to determine the boundary-induced velocity field at position **r** due to the vortex element at position **R** in the presence of the sphere (Ref. 12).

The method introduces a cutoff scale in the Biot-Savart formula which in all results reported here is equal to 1.2 times the discretization length along the vortices. Without this regularization, it is not possible to achieve stable, long-time vortex dynamical evolutions once a particle attaches itself to a vortex.

The method for calculating $\mathbf{V}^b$ was discussed extensively by Kivotides *et al.*[12] We summarize here their method for the sake of completeness. The vortices are discretized into a sequence of N small linear segments **dl**. In this way, the problem is reduced to the evaluation of the boundary-induced correction corresponding to one of these segments $\mathbf{V}^b_{\mathbf{dl}}$, which leads directly to the computation of $\mathbf{V}^b$ by simple summation over the N segments:

$$\mathbf{V}^b = \sum \mathbf{V}^b_{\mathbf{dl}}. \tag{8}$$

By writing $\mathbf{V}^b_{\mathbf{dl}} = \nabla \Phi^b_{\mathbf{dl}}$ and applying the incompressibility constraint $\nabla \cdot \mathbf{V}^b_{\mathbf{dl}} = 0$, we obtain a Laplace equation for $\Phi^b_{\mathbf{dl}}$:

$$\nabla^2 \Phi^b_{\mathbf{dl}} = 0. \tag{9}$$

The solution of this equation must satisfy the boundary condition

$$(\mathbf{V}^s_{\mathbf{dl}} + \nabla \Phi^b_{\mathbf{dl}}) \cdot \hat{\mathbf{n}} = 0, \tag{10}$$

where $\mathbf{V}^s_{\mathbf{dl}}$ is the Biot-Savart velocity associated to the segment **dl**, and $\hat{\mathbf{n}}$ is the unit radial vector field on the surface of the sphere. Due to the linearity of the Laplace equation (9), the solution (subject to boundary conditions) can be computed analytically[12,13] and it reads

$$\Phi^b_{\mathbf{dl}} = \frac{\kappa dl_\perp}{4\pi} \frac{a \sin \phi}{rR} \sum_{n=1}^{\infty} \frac{1}{n+1} \left(\frac{a^2}{rR} \right)^n P_n^1(\cos \theta). \tag{11}$$

In this formula (Fig. 1), $dl_\perp$ is the length of the projection of segment **dl** on the plane that passes through the center of the sphere, O, and is normal to the vector that connects O with the starting point of the segment **dl**, R is the length of the latter vector, and r is the length of the vector that connects O

with the point in space at which the boundary-induced velocity is being computed. In addition, ϕ is the azimuthal angle of the spherical coordinate system attached to the sphere, θ is the polar angle, and $P_n^1(\cos\theta)$ is the associated Legendre function of the first kind, defined by

$$P_n^m(x) = (1-x^2)^{m/2}\frac{d^m P_n(x)}{dx^m}, \tag{12}$$

where $P_n(x)$ is the Legendre polynomial of order n.

Direct differentiation of Eq. (11) gives (for the specific **dl**) the corresponding boundary induced velocity field $\mathbf{V}^b_{\mathbf{dl}}$. The latter is inserted into summation (8) in order to calculate the velocity $\mathbf{V}^b$ that enters Eq. (1). The details of this computation are not trivial and are discussed in great detail in Ref. 12.

With known $\mathbf{V}^s$ and $\mathbf{V}^b$, the evaluation of the right-hand side of Eq. (7) is straightforward. We have used the Gauss quadrature method[26] for the integral over the sphere.

The procedure described above assumes that, at every instant during the evolution of the system, all loops belonging to the vortex link are detached from the particle's surface. In fact formula (11) is valid only in such cases. This severely restricts the usefulness of the method, since, in general, particles attach to vortices.[12] Next, we develop a method that avoids these limitations.

B. Particle-vortex collisions

Reference 12 demonstrated that when a vortex ring approaches a particle at a distance much smaller than the particle diameter, an instability develops and the ring attaches to the sphere. This effect is similar to earlier observations[14,15] of particle-vortex collisions. Assuming that the discretization length dl along the vortex loops is much smaller than the particle diameter, it is plausible to attach to a particle any vortex that approaches it closer than dl. Although, in principle, this appears to be a simple operation, in practice the algorithm that implements it is complex. This is because the algorithm should satisfy the boundary conditions at arbitrarily set numerical accuracy, and in addition, be flexible enough to allow the detachment of vortices from particles. Moreover, the algorithm should allow multiple attachments-detachments taking place simultaneously in dense vortex links. At the same time the algorithm should not jeopardize the stability property of the numerical scheme discussed in the previous section. The method described here overcomes these obstacles and allows routine calculations of particle motion within a system of vortices.

The central idea of the method is to treat vortex-particle collision by adding a number of points to the vortex loop that has collided with the particle. The geometry of the added vortex length is depicted in Fig. 2.

Proposition. The construction of Fig. 2 has the following properties: (a) it complies with the boundary conditions and (b) it embeds the calculation of collision events into the "standard" VD treatment discussed in the previous section.

Proof. To prove part (a), we first put each vortex point into one-to-one correspondence with the vortex segment that ends at this point. Subsequently, we divide the vortex points

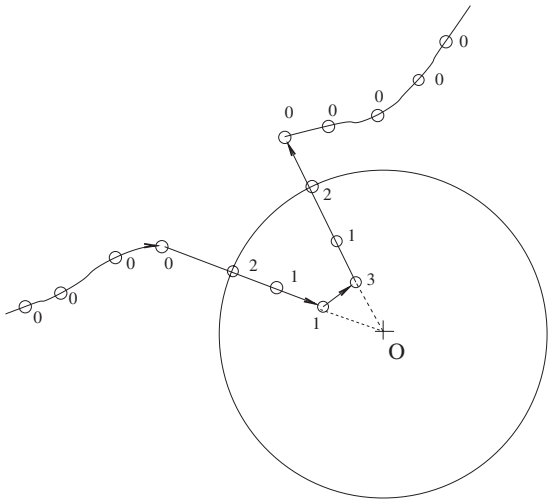

FIG. 2. Typical construction of vortex geometry following the collision of a vortex loop with a particle.

in four categories. Points belonging to the first category, labeled 0-points, lie outside the particle's volume. When a vortex segment defined by two 0-points approaches the particle at a distance smaller than dl, a collision happens and vortex points belonging to the other three categories are (instantaneously) added to the specific vortex loop. Vortex segments corresponding to new points that are labeled 1-points and 2-points are placed (at equal distances dl) along the straight lines connecting the two ends of the colliding segment with the center of the particle (i.e., along particle diameters). The 2-points are placed exactly on the surface of the particle, and the 1-points are placed in the interior of the particle. Finally, new points belonging to a fourth category, labeled 3-points, correspond to segments that form "bridges" (Fig. 2) connecting 1-point segments placed along different particle-radii. Next we show how the boundary conditions can be satisfied by such a construction. We treat each of the four categories of points separately. The segments corresponding to 0-points satisfy the boundary conditions if their boundary induced contribution to the flow is computed by means of Eq. (11) as explained in the previous section. Segments corresponding to 1-points and 2-points do not induce any boundary-associated velocity field, since they are placed along particle diameters and therefore their Biot-Savart velocity field is always tangential to the particle surface. Finally, consider 3-point segments. Their boundary related velocity field can be treated as that of 0-points by replacing formula (11) with an expression appropriate for interior vortex segments derived by Schwarz:[14]

$$\Phi^b_{\mathbf{dl}} = \frac{\kappa dl_\perp}{4\pi}\frac{\sin\phi}{r}\sum_{n=1}^{\infty}\frac{1}{n+1}\left(\frac{R}{r}\right)^n P_n^1(\cos\theta). \tag{13}$$

Notice that the above series converges since R is smaller than r.

To prove part (b) (see also the discussion by Schwarz[14]), we first notice that our geometrical construction does not destroy vortex loops. Precollision loops keep their identity,

simply growing in size. Moreover, the dynamics of 3-points and 1-points need not be considered at all because the part of the vortex loop which lies inside the particle is reconstructed at each time step from the outer vortex configuration (comprised of 0-points). Therefore only 0-points dynamics need to be considered. 0-points evolve because of Biot-Savart interactions with points of all categories, together with accompanying boundary corrections. There is a final issue: does the construction of Fig. 2 guarantee that 2-points move tangentially to the particle surface? We show that this is the case. First, we note that 2-points evolve according to their self-induced velocity and the influence of all other points. However, since 2-points are situated on the particle boundary, and since we have shown in part (a) that our construction satisfies the boundary conditions, we conclude that the velocity of 2-points induced by all other points has zero radial component. Hence we only need to show that the self-induced velocity is along the tangential direction. This is achieved by requiring, first, that the self-induced velocity of a 2-point is identical to the self-induced velocity of the 0-point with which it is connected (there is always one). This is a plausible requirement, since, as discussed by Schwarz,[14] it could be thought that the colliding vortex configuration is always locally normal to the particle surface, i.e., the local vortex geometry is like that of a circular arc normal to the surface of the particle (Fig. 5 of Ref. 14). Thus since our method for the desingularization of the Biot-Savart kernel prescribes that a vortex point's self-induced velocity is that of a vortex ring with radius equal to the local radius of curvature, the two neighboring points (i.e., the 2-point and the 0-point that belong to the aforementioned circular arc) would have the same self-induced velocity, which we choose to be determined by the local radius of curvature at the 0-point. Finally, to complete our argument, we note that, by construction, the latter velocity is along the tangent to the particle's surface, since it must be normal to both vortex segments associated with the 0-point neighboring the 2-point, and one of those segments is one of the particle's diameters.

Remark 1. A simpler alternative to our construction could be one with no 3-points, which happens if the particle's center becomes a vortex point connected directly with the 0-points. Indeed, a similar construction was employed by Schwarz[14] (see his Fig. 20). This method, however, leads to singular particle dynamics originating in the $\frac{\partial \mathbf{V}^s(\mathbf{z},t)}{\partial t}$ term on the right-hand side of Eq. (7), and it is not suitable for our fully dynamical particle-vortex interaction computations.

Remark 2. During complex particle-vortex dynamics, a situation like that of Fig. 3 could appear. In such circumstances, cases where (by accident) a vortex point coincides with the particle's center must be automatically avoided by the algorithm (for the same reasons as those mentioned in Remark 1). The construction of Fig. 2 satisfies this requirement by placing all added points outside a sphere of radius *dl* around the particle's center. In fact, the 3-points were introduced in our method in order to meet precisely this algorithmic contingency. Moreover, by placing the "bridge" segment within discretization-length distance from the center (i.e., as far as possible from the particle's surface), we solve the aforesaid singularity problem with the minimum possible effect on the motion of the vortex-sphere contact points.

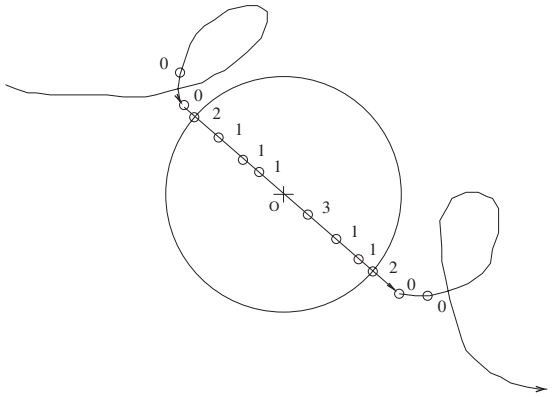

FIG. 3. By placing the "inner-particle" vortex points outside a sphere of typical radius *dl* around the center of the particle, special vortex configurations like the one depicted here cause no pathologies to the computational procedure.

Remark 3. It is well-known that the vortex filament model of superfluid turbulence does not include the physics of collision events. Hence the geometrical construction proposed here belongs (at best) to a family of possible physical models. Contrary to what is stated in Ref. 14, there is an unavoidable arbitrariness in the way the inner-particle vortex geometry dilemma is resolved. One can only plausibly expect that for "reasonable" inner-particle extensions of a colliding loop, the resulting evolution would qualitatively agree with a (hypothetical) GP computation of the same problem which has not been carried out as yet. At a more abstract mathematical level, our solution could be thought of as the VD analog of the construction of physically correct "weak" solutions (e.g., via vanishing viscosity methods) of hyperbolic conservation laws in cases where the "classical" solutions do not exist (e.g., discontinuous wave phenomena in the compressible Euler equations).

IV. SOLUTIONS

The method described above is applied to the problem of particle-vortex collision at finite temperatures. There are three postcollision outcomes: (a) the vortex remains attached to the particle and eventually the vortex-particle compound reaches an equilibrium state (i.e., a stationary particle with a straight vortex attached to it) because of viscous damping, (b) the particle breaks free from the vortex and moves to infinity, and (c) the particle remains in the vicinity of the vortex without being trapped. These are qualitatively very different situations, since in the second case the particle continues its motion and is allowed, for example, to collide with other vortices or to accelerate, extracting kinetic energy from the normal fluid via the Stokes force. In all calculations which we describe, a particle is placed initially at a distance equal to its diameter away from a straight vortex. The particle's initial velocity always aims directly at the vortex. We do a search in a three-dimensional parameter space in order to determine which of the three aforementioned outcomes occurs in each case. The three parameters of the computa-

tional search are (a) the temperature, (b) the particle diameter, and (c) the magnitude of the initial particle velocity. We consider three different temperatures, $T=1.3$, 1.95, and 2.171 K. The corresponding superfluid mass fraction ρ_s/ρ is 0.9550, 0.5182, and 0.0446. We use the same particle diameter $2a=2\times10^{-4}$ cm for all temperatures. For the $T=1.3$ K case, we also compute the motion of a particle of half size, $2a=10^{-4}$ cm. Overall, the computations suggest a generic pattern of particle-vortex collisions. As the particle approaches the vortex, the vortex develops a protruding arc as it tries to avoid the particle. The size of the arc depends on the speed of the approaching particle as well as temperature, since temperature defines, via the magnitudes of the mutual friction force coefficients in Eq. (6), the strength of the nonlinear coupling between particle and vortex. After the formation of the arc, the vortex becomes unstable and impinges upon the particle. Depending on the geometry of the deformed vortex and the particle velocity, the impingement could involve single or multiple attachment events. Notably, for all values of particle speed investigated, the vortex always attaches to the incoming particle.

Once the vortex has attached itself to the particle, there is a number of possible outcomes. For small collision velocities, the particle is trapped by the vortex and subsequently jitters and crawls along it. The direction of this drifting motion depends on the vortex polarity. As the impact velocity of the particle increases, the particle drags the two parts of the vortex (at the expense of its kinetic energy). Equivalently, the vortex moves along the surface of the particle until its two ends find themselves on the "back" side of the particle's surface. At this point, different things can happen. For adequately large particle kinetic energy upon collision, the stretching of the two vortex parts by the particle brings them sufficiently close to each other that a vortex instability develops, and the subsequent reconnection detaches the vortex from the particle (thus the particle breaks free and escapes the vortex neighborhood). For smaller particle kinetic energy values, the particle comes to a halt with the vortex attached to it; subsequently the two parts of the attached vortex move towards the poles of the particle and acquire (because of mutual friction) an equilibrium straight vortex configuration. In a third intriguing case, the particle breaks free from the vortex, but a combination of particle pull and viscous drag brings the particle to a halt in the neighborhood of the vortex. To analyze the influence of viscous drag, we introduce the Stokes time, given by the formula $\tau=a^2\rho_p/3\mu_n$, where ρ_p is the mass density of the particle and μ_n is the dynamic viscosity of the normal fluid. This time is the characteristic time for viscosity to act on the particle in the absence of the vortex. In the considered case, the Stokes time is so small that even very small particle velocities induce a viscous drag strong enough to obstruct any discernible particle motion. Thus the final system configuration consists of a stationary particle close to a stationary (i.e., straight) vortex.

Next, we describe the computations which corroborate the above conclusions. The flow domain is infinite. This choice has a major difficulty from the point of view of computational efficiency: a straight vortex in such a system is necessarily infinite, and thus requires an infinite number of points for its numerical discretization. In order to circumvent this difficulty, we have only computed the VD of a finite portion of the vortex. The vortex extends symmetrically above and below the plane that is normal to the vortex and passes through the initial particle position; the upper end of the vortex is prescribed to continue to its lower end. Such a treatment assumes that the evolved system is adequately large, so that the effects of the unaccounted vortex length on the results are small. Since we can only judge the size of a vortex segment by comparing it with the size of the particle, we have chosen the length of the vortex to be equal to ten particle diameters (i.e., $l_v=2.0\times10^{-3}$ cm). Note that the ratio $l_v/2a$ becomes even greater (thus more favorable) in computations in which we investigate the effect of particle size, which are carried out keeping the vortex length constant, and decreasing the particle size. The vortex length l_v is discretized into 128 elements of length $dl=1.5625\times10^{-5}$ cm. The particle's diameter thus corresponds to approximately 12 grid points, and so vortex deformations close to the surface of the particle are adequately resolved. Moreover, dl is suitable for estimating the particle-vortex proximity that enters the computational algorithms. In computations with half particle size, l_v is discretized into 256 vortex segments so that the resolution quality remains intact. The choice of time step takes into account three processes: (a) the particle velocity, (b) the propagation of Kelvin waves in the system, and (c) the viscous drag. In particular, when computing appropriately dense vortex links, the particles should not propagate by more than a fraction of the intervortex spacing within a time step. This ensures that particle-vortex collisions are adequately resolved. Usually, this concern appears when the normal flow accelerates the particle to high velocities compared to the vortex velocities. The time step δt must not allow the fastest Kelvin wave in the system to propagate by more than one dl in one time step, and must not exceed 0.25τ. The purpose of the prefactor 0.25 is to ensure that the viscous damping process is adequately resolved. For particle diameter $2a=2\times10^{-4}$ cm, the three temperature cases $T=1.3$, 1.95, and 2.171 K correspond to $\tau=3.1935\times10^{-5}$, 3.43×10^{-5}, and 1.91×10^{-5} s, respectively. In the computations reported here, typical time steps vary between $\delta t=3.15\times10^{-8}$ and 1.95×10^{-11} s. Using the previously described methods and the aforementioned spatial and temporal grid sizes, there were no problems with numerical stability. Finally, one needs to ensure that the zero radial velocity boundary conditions on the surface of the particle are enforced with great accuracy throughout the computation. If the boundary condition was enforced exactly, at all points on the particle's surface the total velocity vector would form a 90° angle with the radial direction vector. We allow small computational deviations from this exact condition only up to a given tolerance typically from 0.01° to 0.1°. This is achieved with a modest number of terms in the Legendre expansion, of the order of 100 (see also Ref. 12 for additional technical details).

We define the escape particle velocity as the initial velocity for which a particle, initially at a distance from the straight vortex equal to the diameter, breaks free from the vortex and moves to infinity. The results for the escape velocity are summarized in Table I. It is evident that, for fixed particle size, there is strong temperature dependence. Noting

TABLE I. Escape initial particle speed V_e for three different temperatures, $T=1.3$, 1.95, and 2.171 K. We have considered two particle diameters, $2a=2\times10^{-4}$ and 10^{-4} cm, in order to investigate the effects of particle size. In all cases, the initial vortex-particle distance is equal to the particle diameter.

Temperature T (K)	Diameter $2a$ (cm)	Escape velocity V_e (cm/s)
1.3	10^{-4}	45
1.3	2×10^{-4}	24
1.95	2×10^{-4}	31
2.171	2×10^{-4}	76

that at temperature $T=1.3$ K a particle of diameter $2a=2\times10^{-4}$ cm escapes when it has initial velocity $V_e=24$ cm/s, and that a particle of diameter $2a=10^{-4}$ cm escapes when it has initial velocity $V_e=45$ cm/s, it appears that the escape velocity is approximately inversely proportional to the diameter of the particle. Care is needed in interpreting this result. One must take into account that the minimal escaping initial kinetic energy of the smaller particle is approximately half of the minimal escaping initial kinetic energy of the larger particle, that the damping time τ for the larger particle is four times larger than that of the smaller particle, and, finally, that the latter starts its motion towards the vortex at a distance half of the initial distance of the former. For the larger particle the "damping" distance is $s_d=V_e\tau=1.908\times10^{-4}$ cm which is approximately equal to the original distance (one diameter) of the particle from the vortex. For the smaller particle $s_d=0.894\times10^{-4}$ cm, which, again, is close to the initial particle-vortex distance. Certainly, it must also be taken into account that viscous damping is only one of the forces acting on the particle, whereas the computed results incorporate all the various physical ingredients of our model. On the other hand, the increase of the escaping velocity with temperature appears to be a direct consequence of the larger damping effects at higher temperatures (the decrease of the damping time τ and the increase of the mutual friction parameters).

Figure 4 shows a sequence of particle-vortex configurations depicting the collision of a particle of diameter $2a=2\times10^{-4}$ cm with a vortex at $T=1.3$ K. The initial particle velocity magnitude is $V=25$ cm/s. Figure 4(a) shows that the vortex is deformed as it tries to avoid the incoming particle. The collision excites Kelvin waves [Figs. 4(b) and 4(c)] that propagate along the vortex as the latter moves towards the "back" side of the particle [Fig. 4(c)]. Figure 4(d) depicts the particle dragging the vortex, forcing its two parts to come together, thus facilitating a particle-vortex detachment. Following the detachment, the vortex recoils [Fig. 4(e)], and the subsequent relaxation creates more Kelvin waves along the vortex [Fig. 4(f)]. It should be noted that for this particular polarity (the vorticity vector points upwards) the vortex forms a protruding bump "rightwards" with respect to an observer moving with the particle. This is also the direction of postcollisional particle deflection [Fig. 4(d)]. This could be understood intuitively by observing that the collision site of the particle represents a low pressure flow region due to

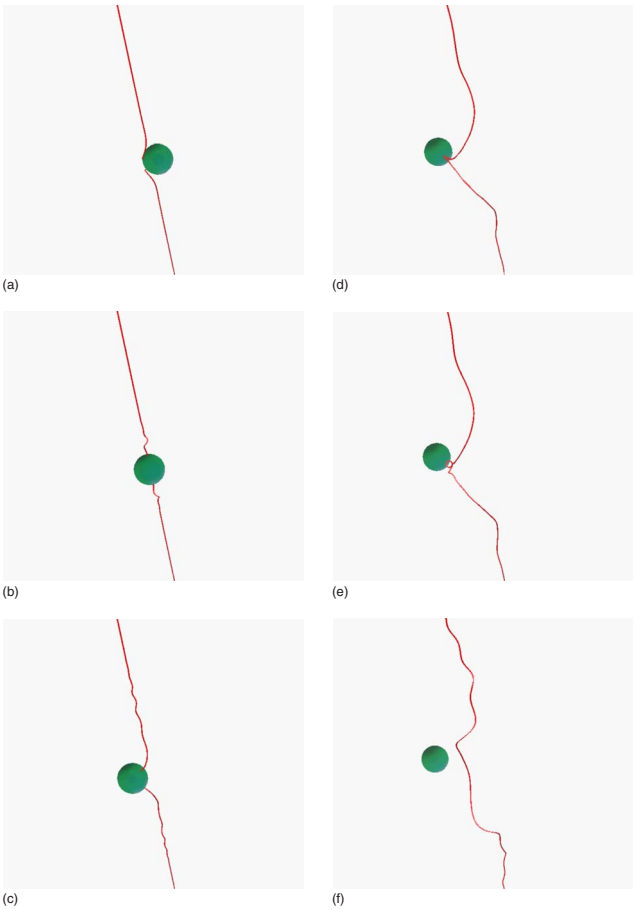

FIG. 4. (Color online) Particle-vortex collision for initial particle speed $V=25$ cm/s, at $T=1.3$ K. Time increases as follows: $t_a=0.6309\times10^{-5}$ s (a), $t_b=0.9464\times10^{-5}$ s (b), $t_c=0.1577\times10^{-4}$ s (c), $t_d=0.4416\times10^{-4}$ s (d), $t_e=0.5047\times10^{-4}$ s (e), and $t_f=0.7887\times10^{-4}$ s (f). The particle arrives from the right. The particle diameter is $2a=2\times10^{-4}$ cm, and the initial particle-vortex distance is $2a$. The particle attaches to the vortex, and, after stretching it, breaks free.

the attached vortex segments. Since nothing analogous occurs at the opposite side of the particle, a net, deflecting pressure force aiming towards the collision site is expected. Figure 5 (left) analyzes the contributions to the total force acting on the particle. Notably, the boundary-induced force, $\mathbf{f_b}=\frac{1}{2}\rho_s\int_S dS\ (\mathbf{V}^s+\mathbf{V}^b)^2\hat{\mathbf{n}}$, is of minor importance and contributes significantly to the dynamics only at times close to the collision time (i.e., $t_1=0.6309\times10^{-5}$ s). In comparison, the damping force, $\mathbf{f_d}=6\pi a\mu_n(\mathbf{V}^n-\mathbf{V}^p)$, is the strongest during the initial stages of evolution (indicating that the initial distance is so large that the boundary-induced force has no effect on the particle motion). Once the collision occurs, the local force, $\mathbf{f_l}=2\pi\rho_s a^3\partial\mathbf{V}^s(\mathbf{z},t)/\partial t$, becomes the dominant one, due to the generation and propagation of Kelvin waves along the vortex. It is expected that at higher temperature, increased damping of Kelvin waves due to mutual friction would diminish the importance of $\mathbf{f_l}$ at higher temperatures. After the particle breaks free from the vortex, its dynamics are dominated by viscous damping. This observation, in conjunction with the prescribed zero normal fluid velocity, ex-

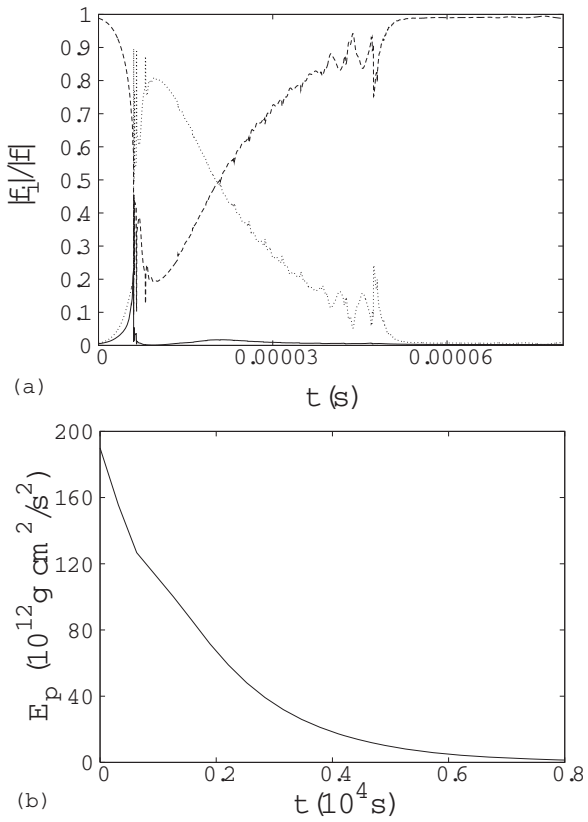

FIG. 5. Same particle-vortex collision as in Fig. 4. The top graph shows relative contributions $\mathbf{f_i}$ $(i=d,l,b)$ to the magnitude of the total force acting on the particle due to damping, $\mathbf{f_d}$, local, $\mathbf{f_l}$, and boundary-induced force, $\mathbf{f_b}$. The contributions are normalized by the magnitude of the total force, $|\mathbf{f}|$. The boundary-induced force (bottom, solid line) is of importance only during the initial collision times (see the small spike at the bottom of the graph for $t \approx 0.000\,01$ s). The damping force (dashed line) dominates both the initial and final stages of evolution. The local force (dotted line) is initially zero but builds up quickly. The bottom graph shows the kinetic energy of the particle versus time.

plains (Fig. 5, right) the decrease of the particle velocity after its detachment from the vortex. Note in Fig. 5 (right) the change in the slope of particle's kinetic energy $E_p = 0.5 m_p V_p^2$ at the onset of collision. The lack of smoothness is due to the discrete nature of the model. Our previous computations[10,11] showed that viscous damping forces the particles to move with the normal fluid velocity in between their collisions with the vortices. In that work, we argued that the particle velocity could be a very good indicator of the normal fluid velocity, provided that particles are not arrested by the superfluid vortices. The present findings suggest that an experiment (involving necessarily a dilute system of particles) could make use of this result by ensuring that the normal fluid velocity (hence also the particles velocity) is larger than the escape velocity reported here.

A second computation is carried out at $T=1.3$ K with initial particle velocity $V=20$ cm/s. In this case, Fig. 6, the particle is arrested by the vortex. The mechanism is as follows. The particle attaches to the vortex and turns as before [Fig. 6(a)], but its kinetic energy is not sufficiently large to stretch the vortex and "force" a detachment (as in Fig. 4).

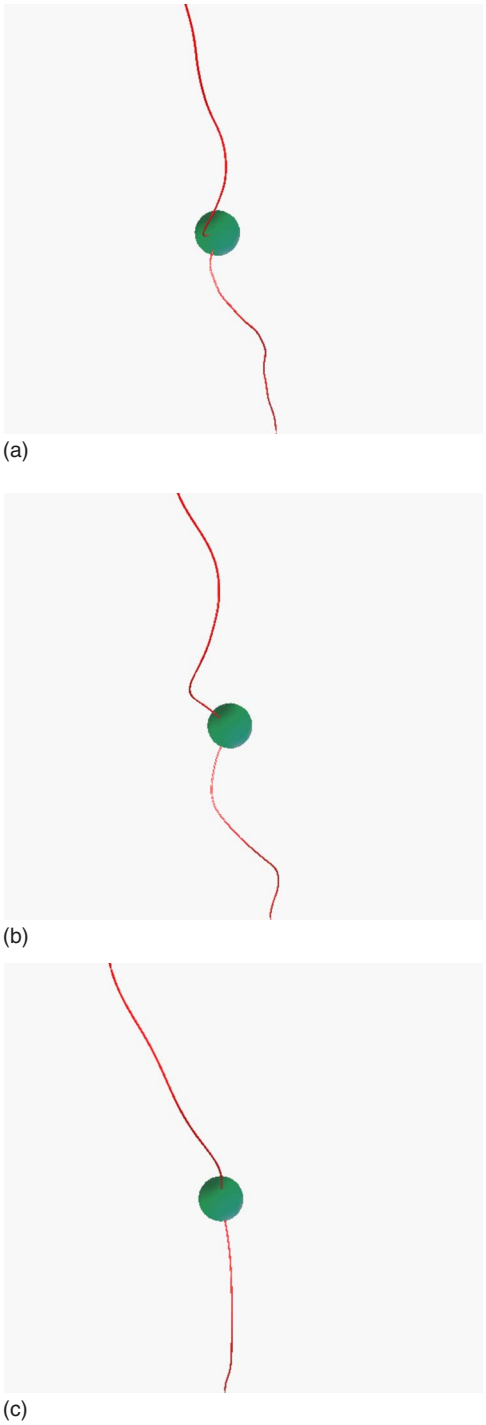

FIG. 6. (Color online) Particle-vortex collision for initial particle speed $V=20$ cm/s, at $T=1.3$ K. Time increases as follows: $t_a = 0.4732 \times 10^{-4}$ s (a), $t_b = 0.8833 \times 10^{-4}$ s (b), and $t_c = 0.5047 \times 10^{-3}$ s (c). The particle has arrived at the vortex from the right. The particle diameter is $2a = 2 \times 10^{-4}$ cm, and the initial particle-vortex distance is $2a$. After colliding with the vortex, the particle slows down and stops, since it lacks the necessary kinetic energy to stretch the vortex and induce a detachment.

Instead, the particle turns further, following a circular trajectory [Fig. 6(b)]. In the meantime, the vortex also moves back and forth along the surface of the sphere and develops long

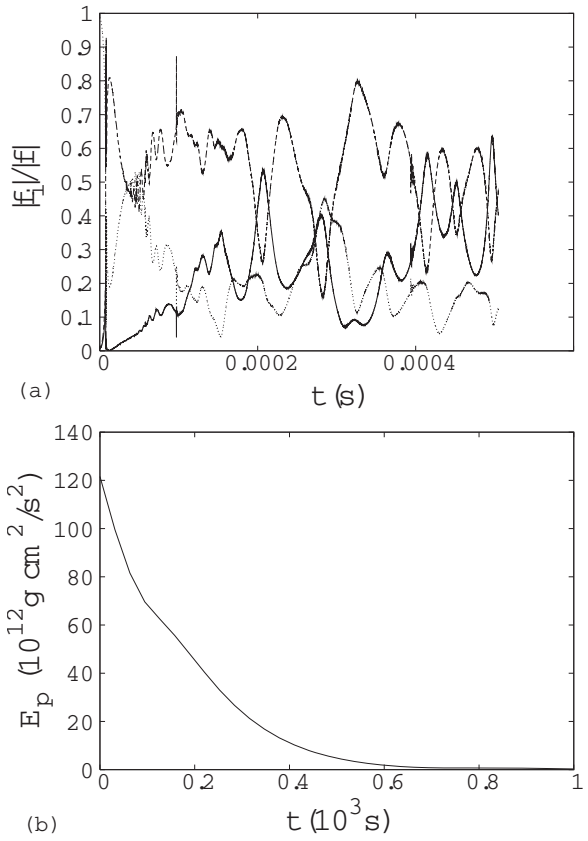

FIG. 7. Same particle-vortex collision as in Fig. 6. The top graph shows contributions to the magnitude of the total force acting on the particle due to damping, $\mathbf{f_d}$ (dotted, bottom line for large t), local, $\mathbf{f_l}$ (dashed, top line), and boundary-induced force, $\mathbf{f_b}$ (solid line). The contributions are normalized by the magnitude of the total force. Unlike Fig. 5, all contributions are of comparable importance, without any particular one dominating the others. The bottom graph shows the evolution of the particle's kinetic energy versus time.

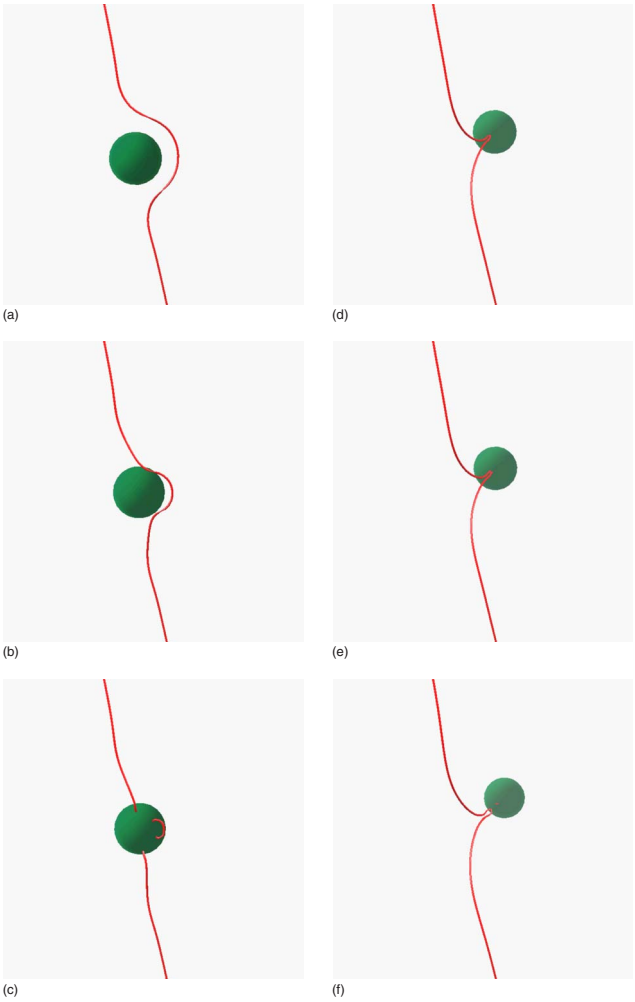

FIG. 8. (Color online) Particle-vortex collision for initial particle speed $V=200$ cm/s, at $T=2.171$ K. Time increases as follows: $t_a=0.9465\times10^{-6}$ s (a), $t_b=0.1230\times10^{-5}$ s (b), $t_c=0.1325\times10^{-5}$ s (c), $t_d=0.4069\times10^{-5}$ s (d), $t_e=0.4164\times10^{-5}$ s (e), and $t_f=0.5678\times10^{-5}$ s (f). The particle arrives from the left. The particle diameter is $2a=2\times10^{-4}$ cm, and the initial particle-vortex distance is $2a$. Note that the vortex attaches at the particle's surface at four points [as in (c)], forming a vortex "handle." Note also the nontrivial mechanism of vortex detachment from the surface; (d) the vortex detaches from the particle; (e) the particle moves slow enough for the vortex to attach to it again via a new instability-induced collision; and (f) after numerous collisions, the particle finally escapes the vortex.

wavelength waves [Fig. 6(b)] that, in due time, are damped [Fig. 6(c)]. In the final configuration, both vortex and particle have zero velocities. Figure 7 (left) shows the contributions to the forces on the particle. They look very different from the case of initial velocity $V=25$ cm/s. The arrest of the particle by the vortex leads to time dependent vortex configurations that explain the dominating role of the local force $\mathbf{f_l}=2\pi\rho_s a^3\partial\mathbf{V}^s(\mathbf{z},t)/\partial t$ (upper line in the graph). In opposition to the $V=25$ cm/s case, the boundary induced force $\mathbf{f_b}=\frac{1}{2}\rho_s\int_S dS\ (\mathbf{V}^s+\mathbf{V}^b)^2\hat{\mathbf{n}}$ makes significant contributions to the dynamics, and, at later evolution times, is even more important than the damping force $\mathbf{f_d}=6\pi a\mu_n(\mathbf{V}^n-\mathbf{V}^p)$. A monotonically decreasing particle kinetic energy E_p is depicted in Fig. 7 (right). According to the graph, the particle halts at $t\approx8\times10^{-4}$ s.

It is useful to compare the particle-vortex collision phenomenology at $T=1.3$ K with what happens at other temperatures. Figure 8 shows the collision of a particle of diameter $2a=2\times10^{-4}$ cm and initial velocity $V=200$ cm/s with a vortex (initially) placed at distance $2a$ away, when the temperature is $T=2.171$ K. Under these conditions, the vortex and the particle eventually separate. One notices the pronounced deformation of the vortex, which forms a bump, comparable to the size of the particle [Fig. 8(a)]. Due to the combined action of the Biot-Savart law, and boundary and mutual friction effects, the bump collapses [Fig. 8(b)] onto the surface of the particle creating a characteristic arc [Fig. 8(c)]. Because of mutual friction, the arc shrinks continuously until its two "legs" annihilate each other. The particle-vortex detachment occurs in a special way: the particle stretches the vortex and two almost parallel vortex segments are formed behind the particle. Due to continuous stretching, these two segments approach each other until they reconnect, and the particle detaches from the vortex [Fig. 8(d)]. How-

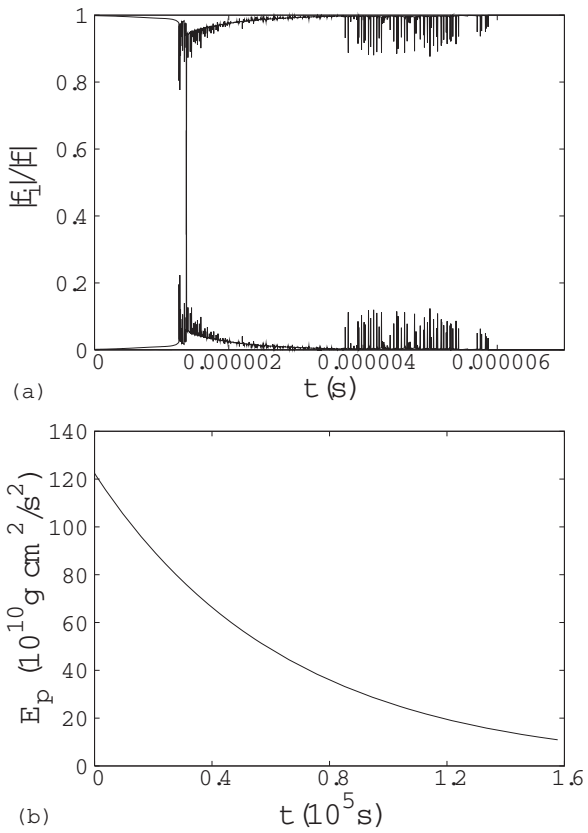

FIG. 9. Same particle-vortex collision as in Fig. 8. The top graph shows contributions to the magnitude of the total force acting on the particle due to damping, $\mathbf{f_d}$, local, $\mathbf{f_l}$, and boundary-induced force, $\mathbf{f_b}$. The contributions are normalized by the magnitude of the total force. The boundary-induced force is always negligible compared to the other two forces, and is not even discernible in the graph. The damping force dominates at all times. The bottom graph shows the evolution of the particle kinetic energy versus time.

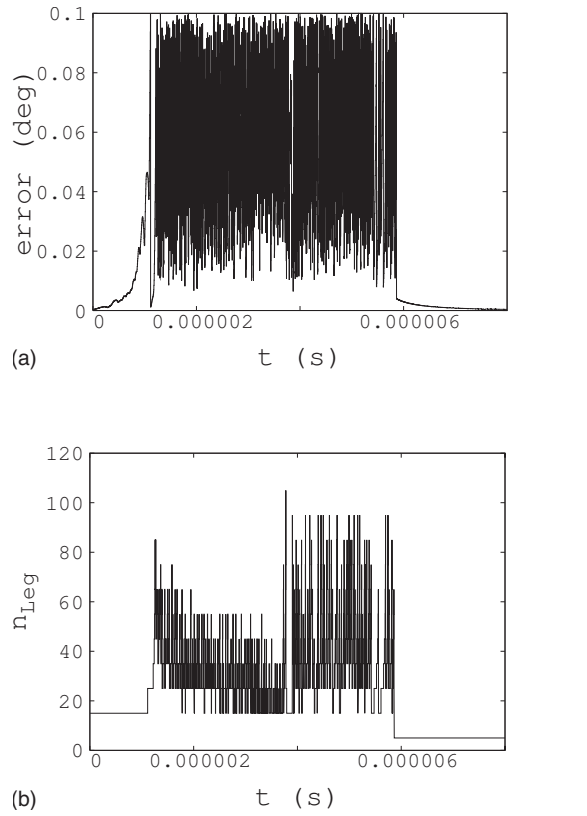

FIG. 10. Particle-vortex collision at $T=2.171$ K. The initial particle speed is $V=200$ cm/s, its diameter is $2a=2\times10^{-4}$ cm, and the initial particle-vortex distance is $2a$. The top graph shows that, throughout the evolution, the angle between the total superfluid velocity and the normal radial vector to the surface remains bounded below 0.1°. The bottom graph shows the order of the Legendre functions that is needed at each time step in order to maintain this accuracy.

ever, because of small particle-vortex separation velocity, the vortex remains sufficiently close to the particle so that a subsequent collision reattaches the vortex to the particle [Fig. 8(e)]. This phenomenon occurs numerous times until [Fig. 8(f)], eventually, the particle breaks free. Notice that throughout the system's evolution, the vortex contour remains very smooth due to strong mutual friction damping of any excited Kelvin waves.

A natural question arises: Is it possible, that for sufficiently high approaching velocities, the boundary-induced deformation of the vortex is so large that the particle altogether "misses" the vortex? In order to clarify this matter, we have gradually increased the initial particle velocity, achieving a (purely hypothetical) particle speed of $V=600$ m/s. We have found that (in all cases) the particle-vortex collision pattern is very similar to that in Fig. 8, i.e., the particle always collides with the vortex. This appears to be so, because the "collapse" of the aforementioned bump onto the particle surface happens at time scales smaller than the time necessary for the particle to escape the neighborhood of the vortex.

Figure 9 (left) shows the contributions to the particle's total force. Due to the high velocities involved, the damping force, $\mathbf{f_d}=6\pi a\mu_n(\mathbf{V}^n-\mathbf{V}^p)$, is dominant throughout the evolution. This is reflected by the particle kinetic energy E_p evolution shown in Fig. 9 (right) that shows no noticeable effect arising from the attaching-detaching processes. The only other force of some importance is the local force, $\mathbf{f_l}=2\pi\rho_s a^3\partial\mathbf{V}^s(\mathbf{z},t)/\partial t$, that becomes significant only after collision events. In particular, Fig. 9 (left) shows that the importance of $\mathbf{f_l}$ (lower line in the graph) attains a peak at the onset of the first attaching collision before it starts decaying as the particle stretches the vortex. The decay continues until the system's evolution arrives at the aforementioned regime of multiple attaching-detaching processes, which correspond to the revival of the importance of the $\mathbf{f_l}$ force at later times. Overall, as anticipated in the discussion of the $T=1.3$ K results, the strong mutual friction damping for $T=2.171$ K diminishes the (relative) strength of $\mathbf{f_l}$. The collision shown in Fig. 8 is the most difficult to calculate. Hence it is very appropriate for discussing the accuracy and efficiency of our method. We define the computational error as the angle away from 90° between the superfluid velocity and the normal radial vector to the surface integrated over the sphere. As shown in Fig. 10(left), the computation is very accurate, since throughout the evolution the absolute error never exceeds one-tenth of a degree. We have verified that the error

could be made arbitrarily small (subject to round-off error limits) by increasing the number of Legendre functions. Also shown in Fig. 10(right) is the order of Legendre functions that need to be taken into account (at each time step) in order to achieve the desired accuracy during the evolution. At most 100 functions are needed. Note that the required Legendre function order decreases, until, around $t=4\times10^{-6}$ s, it suddenly increases again. This increase corresponds to the recurring detachment-attachment processes described above [Figs. 8(d) and 8(e)]. It is notable that, although the vortex connects twice with the particle upon collision developing a "handle"-like structure, even this case does not require many Legendre functions. The sharp decrease of the number of the required Legendre functions around $t=6\times10^{-6}$ s corresponds to the final particle-vortex detachment.

Figure 11 depicts the effect of strong mutual friction damping on the dynamics of an arresting particle-vortex collision for $T=2.171$ K. It is observed that, despite the collision, there is no evidence of Kelvin waves on the vortex. The vortex (left graph) is almost straight, and its two parts are never stretched strongly enough to meet and reconnect again. Instead, the vortex moves towards the poles of the particle, and straightens up (right graph). This effect is accompanied by the loss of all particle kinetic energy. Hence the system reaches a configuration in which the particle and the vortex are at rest, although the fluid is moving according to a perturbed potential vortex velocity field.

Figure 12 shows a remarkable case of particle-vortex collision, when $T=1.95$ K, $2a=2\times10^{-4}$ cm, $V=31$ cm/s, and initial particle-vortex distance is equal to $2a$. Although the particle escapes the vortex, it comes to a halt a few diameters away from it. We have continued the calculation until $t_e=0.551\times10^{-1}$ s which is two orders of magnitude larger than the approximate halting time ($t_4=0.6309\times10^{-3}$ s in Fig. 12) and corresponds to approximately 2×10^6 time steps. We verified that the particle did not fall into the vortex, remaining static even after times large compared with the duration of the collision. This phenomenon can be explained by observing the balance of the forces contributing to the motion of the particle in Eq. (7). Figure 13(left) shows that although the local force $\mathbf{f_l}=2\pi\rho_s a^3\partial\mathbf{V}^s(\mathbf{z},t)/\partial t$ is important as long as the particle remains attached to the vortex, it eventually falls off to zero following particle-vortex detachment. On the other hand, the damping force $\mathbf{f_d}=6\pi a\mu_n(\mathbf{V}^n-\mathbf{V}^p)$ remains of importance throughout the evolution of the system, and is responsible for halting the particle by (eventually) counterbalancing the boundary-induced force $\mathbf{f_b}=\frac{1}{2}\rho_s\int_S dS\,(\mathbf{V}^s+\mathbf{V}^b)^2\hat{\mathbf{n}}$. The latter force is not as significant as the other two forces during the collision phase, but becomes important, after particle-vortex detachment, when the Kelvin waves are damped and the vortex starts straightening up. The kinetic energy of the particle E_p decreases monotonically to zero. Notice the discontinuity in the slope that corresponds to the attaching collision. Overall, it appears that, in cases where the particle halts at sufficient distance from the vortex, the boundary-induced force could be so small that an appropriately small damping time τ could create an exactly canceling damping force even for negligible particle velocities. In this way, the particle moves so slowly that its motion is undetected even after large compared to the duration of the collision times. To confirm this, we have performed a second calculation in which the Stokes force was removed from the particle equation of motion after the approximate halting time t_4. It was then observed that the boundary-induced force pulls the particle towards the vortex. This intriguing phenomenon (the particle halting away from the vortex) was also observed in a separate calculation with the same temperature and particle size but initial velocity $V=35$ cm/s.

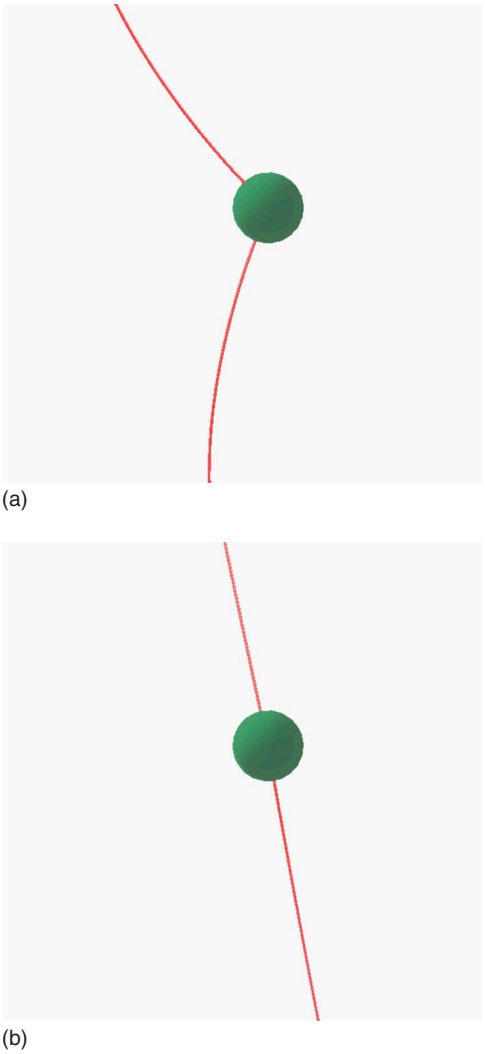

FIG. 11. (Color online) Particle-vortex collision for initial particle speed $V=75$ cm/s at $T=2.171$ K. Time increases as follows: $t_a=0.1515\times10^{-3}$ s (a) and $t_b=0.3405\times10^{-3}$ s (b). The particle has arrived from the left. The particle diameter is $2a=2\times10^{-4}$ cm, and the initial particle-vortex distance is $2a$. The particle is brought to a halt after its collision with the vortex. As seen on the top graph, the two arresting vortex segments initially straighten up before migrating towards the poles of the particle, where (bottom graph) they align with the vertical diameter acquiring a static configuration.

Remark 4. By comparing the solutions presented in this work with realistic laboratory and natural flow situations, some modeling approximations become apparent. The most obvious has to do with the size of the computational domain. In actual flows, the length of the superfluid vortices is many

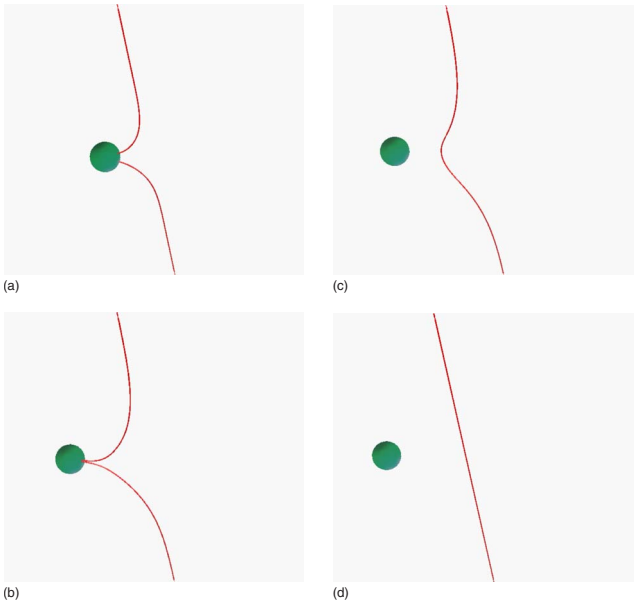

FIG. 12. (Color online) Particle-vortex collision for initial particle speed $V=31$ cm/s, at $T=1.95$ K. Time increases as follows: $t_a=0.2208\times10^{-4}$ s (a), $t_b=0.5678\times10^{-4}$ s (b), $t_c=0.6940\times10^{-4}$ s (c), and $t_d=0.6309\times10^{-3}$ s (d). The particle has arrived from the right. The particle diameter is $2a=2\times10^{-4}$ cm, and the initial particle-vortex distance is $2a$. The particle escapes the vortex but it halts a few particle diameters away from it. It remains static as the vortex relaxes towards a straight line configuration.

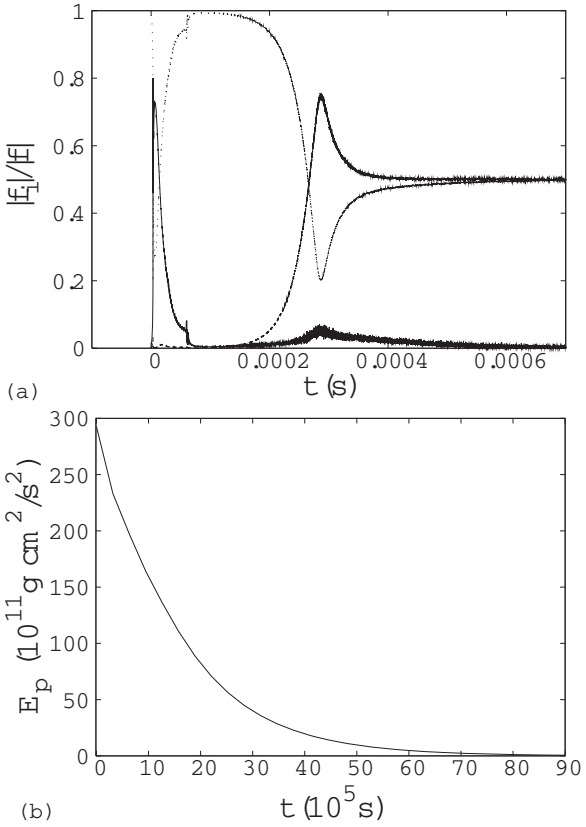

FIG. 13. Particle-vortex collision for initial particle speed $V=31$ cm/s, at $T=1.95$ K. The particle diameter is $2a=2\times10^{-4}$ cm, and the initial particle-vortex distance is $2a$. The top graph shows contributions to the magnitude of the total force acting on the particle due to damping, $\mathbf{f_d}$, local, $\mathbf{f_l}$, and boundary-induced, $\mathbf{f_b}$, forces. The contributions are normalized by the magnitude of the total force. The damping force (dotted line) dominates at early times, and is eventually balanced by the boundary-induced force (dashed line). The local force (solid line) is important during collision only, and falls off to zero as the particle halts (Fig. 12). The bottom graph shows the evolution of the particle's kinetic energy.

orders of magnitude larger than the size of the particles (instead of a single order of magnitude as it is here). This limitation is more important for low temperatures. In a long straight vortex, the collision induced Kelvin waves propagate away from the collision region, and their continuous excitation is as important a damping mechanism of particle motion as is the viscous damping. In the smaller model system employed here, the Kelvin waves, due to the particular boundary conditions, interfere at the respective ends of the computational vortex domain, and then reenter the latter, before colliding with the particle depositing some of their energy on it. At higher temperatures this phenomenon becomes less important due to mutual friction-induced Kelvin wave damping. Thus higher temperature results are more reliable for use in interpreting experiments, while the low temperature results might underestimate the required initial escape velocity. Other difficulties have to do with the lack of a self-consistent account of the interaction between the normal fluid and the particle, as well as between the normal-fluid and the superfluid. Finally, the straight vortex configuration which we considered is idealized compared to the complex turbulent counterflow situations that are experimentally studied. Certainly, these issues need to be addressed in the future. Their full resolution requires nontrivial mathematical developments in this topic.

V. CONCLUSIONS

We have presented a numerical, computational, and physical analysis of particle-vortex collisions in thermal superfluids. Using our method, we have shown that there is a critical incoming particle velocity above which the particle and the vortex separate after their collision. This critical velocity is proportional to the fluid temperature and inversely proportional to the particle size. In connection with the findings of Ref. 10, these results corroborate the possibility of direct measurement of normal fluid velocity in thermal superfluids via appropriately designed particle image velocimetry (PIV) experiments. In particular, the authors of Ref. 10 have shown that, when a particle moves in between a dilute vortex link, the Stokes drag causes it to move with the normal fluid velocity. However, it was not clear what happens when a particle collides with a vortex. If the particle is trapped by the vortex, a PIV measurement of the normal fluid velocity would become invalid at the onset of collision. However, the present results indicate that the particle can escape the vortex (see Table I), and once free, it will (as shown in Ref. 10) be forced by the Stokes drag to move once again with the normal fluid velocity. In this way, a hypothetical PIV measurement of the particle velocity would record the normal fluid

velocity most of the time with the exception of small time periods centered around particle-vortex collision events. The duration of the latter events could be made as small as desired by diluting the vortex system and/or by increasing the particle velocity. According to the above, particle insertion into very dense counterflow vortex tangles is not the best approach to measure the normal fluid velocity. This is because, as it was shown by counterflow measurements,[27,28] the particles do not move with the normal flow velocity in such flows. According to the present findings, experiments with dilute vortex systems could be more successful in this respect.

ACKNOWLEDGMENT

This research was supported by EPSRC Grant No. GR/T08876/01.

[1] *Quantized Vortex Dynamics and Superfluid Turbulence*, edited by C. F. Barenghi, R. J. Donnelly, and W. F. Vinen (Springer, Berlin, 2001).
[2] A. P. Finne, V. B. Eltsov, R. Hanninen, N. B. Kopnin, J. Kopu, M. Krusius, M. Tsubota, and G. E. Volovik, Rep. Prog. Phys. **69**, 3157 (2006).
[3] W. F. Vinen and J. J. Niemela, J. Low Temp. Phys. **128**, 167 (2002).
[4] D. Kivotides, Phys. Rev. Lett. **96**, 175301 (2006).
[5] D. Kivotides, Phys. Lett. A **326**, 423 (2004).
[6] D. Kivotides, J. C. Vassilicos, C. F. Barenghi, and D. C. Samuels, Europhys. Lett. **57**, 845 (2002).
[7] T. Zhang and S. W. Van Sciver, Nat. Phys. **1**, 36 (2005).
[8] G. P. Bewley, D. P. Lathrop, and K. R. Sreenivasan, Nature (London) **44**, 588 (2006).
[9] D. R. Poole, C. F. Barenghi, Y. A. Sergeev, and W. F. Vinen, Phys. Rev. B **71**, 064514 (2005).
[10] D. Kivotides, C. F. Barenghi, and Y. A. Sergeev, Phys. Rev. Lett. **95**, 215302 (2005); Y. A. Sergeev, S. Wang, E. Meneguz, and C. F. Barenghi, Low Temp. Phys. **146**, 417 (2007).
[11] D. Kivotides, C. F. Barenghi, and Y. A. Sergeev, Europhys. Lett. **73**, 733 (2006).
[12] D. Kivotides, C. F. Barenghi, and Y. A. Sergeev, J. Low Temp. Phys. **144**, 121 (2006).
[13] K. W. Schwarz, Phys. Rev. A **10**, 2306 (1974).
[14] K. W. Schwarz, Phys. Rev. B **31**, 5782 (1985).
[15] M. Tsubota and S. Maekawa, Phys. Rev. B **47**, 12040 (1993).
[16] N. V. Brilliantov and T. Poschel, *Kinetic Theory of Granular Gases* (Oxford University Press, Oxford, 2004).
[17] A. J. Chorin, *Vorticity and Turbulence* (Springer, Berlin, 2006).
[18] D. A. Drew and S. L. Passman, *Theory of Multicomponent Fluids* (Springer, Berlin, 2004).
[19] O. C. Idowu, D. Kivotides, C. F. Barenghi, and D. C. Samuels, J. Low Temp. Phys. **120**, 269 (2000).
[20] C. F. Barenghi, R. J. Donnelly, and W. F. Vinen, J. Low Temp. Phys. **52**, 189 (1983).
[21] D. Kivotides, C. F. Barenghi, and D. C. Samuels, Europhys. Lett. **54**, 774 (2001).
[22] B. E. Griffith and C. S. Peskin, J. Comput. Phys. **208**, 75 (2005).
[23] R. R. Nourgaliev, T. N. Dinh, and T. G. Theofanous, J. Comput. Phys. **213**, 500 (2006).
[24] N. G. Berloff and P. H. Roberts, Phys. Rev. B **63**, 024510 (2000).
[25] G. S. Winckelmans and A. Leonard, J. Comput. Phys. **109**, 247 (1993).
[26] W. H. Press, B. P. Flannery, S. A. Teukolsky, and W. T. Vetterling, *Numerical Recipes in FORTRAN: The Art of Scientific Computing* (Cambridge University Press, Cambridge, England, 1992).
[27] T. Zhang, D. Celik, and S. W. Van Sciver, J. Low Temp. Phys. **134**, 985 (2004).
[28] Y. A. Sergeev, C. F. Barenghi, and D. Kivotides, Phys. Rev. B **74**, 184506 (2006).